Pharaonic Journal of Science
https://pjscience.org/
PJS
SPBH

Creating and Analysing Electronic Well-Log Patterns for Identifying Environmental Facies in Abu-Roash 'G' Member, West Qaroun field, and Northern Western Desert, Egypt

Mohie Eldin Khaled Saber [a], Fathy Hassan Mohamed [b], Ahmed Moustafa El-Sabbagh [b], Salah Abbas Omar [c], Mohamed Mahmoud Abd Elrahman [d].

(a) Petroleum Geology Department, Faculty of Science, Alexandria University, Alexandria, 21568, Egypt.
(b) Geology Department, Faculty of Science, Alexandria University, Alexandria, 21568, Egypt
(c) Technical Manager in DATALOG Oil Services Company
(d) Senior Reservoir Engineer in Sahara Oil and Gas

E-Mails: Mohie1222@gmail.com, fathi.hassan@alexu.edu.eg, ahmed.elsabbagh@alexu.edu.eg, salah.omar.057@gmail.com, m.mahmoud1311@gmail.com

DOI: 10.71428/PJS.2025.0212

ABSTRACT

This study highlights the challenges of exploring oil in the Abu Roash 'G' Member, within Egypt's Abu Gharadig Basin. The reservoir is formed in a near-shore depositional environment and is highly heterogeneous, with rock properties varying dramatically over short distances. Analysing the provided logs is essential in providing correlations, and visualizing those correlations is crucial for understanding the environmental characteristics and spatial changes between the wells. Creating patterns using electronic well-logs helps with identifying facies, and that, in turn, can be used while correlating.

Keywords: Abu Gharadig Basin, Abu Roash 'G', Facies, Environment, Well-Logs Patterns

1. Introduction

Exploring oil from the Abu Roash 'G' Member in the Abu Gharadig basin is one of the main challenges for exploration and development, since it is a very heterogeneous reservoir of shale, carbonate, and sand intercalations. In the West Qarun area, the primary trapping mechanisms are tilted fault blocks and faulted anticlines. Sahara Oil & Gas has inferred the potential for combination traps and stratigraphic traps (1). The West Qarun concession is established in the Northern part of the Western Desert of Egypt, near the convergence boundary of three tectonic plates (Euroasian, African, and Arabian) and the Nile Delta region, about 200 km Southwest of Cairo city. The West Qarun concession is impacted by the creation of the Red Sea and its branches (Gulfs of Suez and Aqaba). The block holds an area of 46.2 km^2 and includes the West Qarun oil field (Fig.1). Production began in October 1994.

Seven smaller members (from A to G) compose the Abu Roash Formation; they are considered to be of the early Senonian, Turonian, and late Cenomanian age. Furthermore, the Abu Roash 'G' Member could also be segmented into Upper, Middle, and Lower units, indicating three different depositional cycles (2). According to the Egyptian General Petroleum Corporation (3), the Abu Roash 'G' Member is a major reservoir for both oil and gas plays. The Abu Roash 'G' Member overlies conformably the Bahariya Formation. It is composed of limestone and shale, with interbeds of sandstone (4).

Received: August 5, 2025. Accepted: October 25, 2025. Published: November 15, 2025

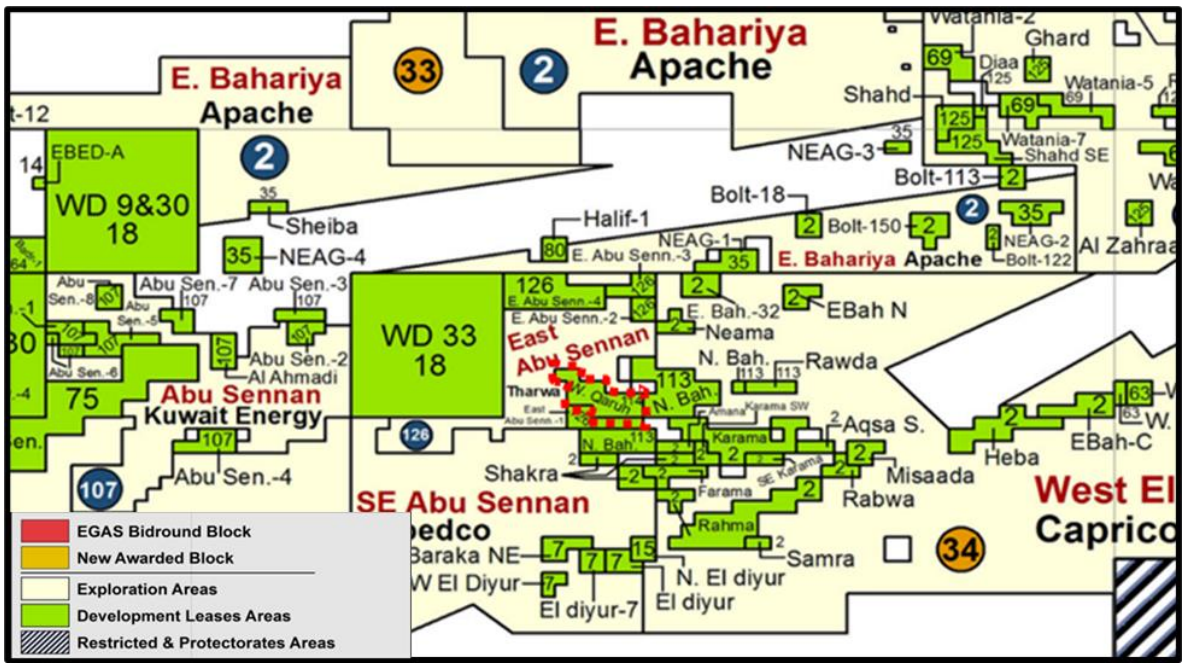

Fig. 1. The West Qarun field highlighted with red dots, with the concession number of 114 (5).

The main productive horizon in the West Qarun field is the Abu Roash 'G' Member. The Abu Roash 'G' Member could be subdivided structurally into two parts in this field. The southern part is characterized by a gentle dip. The northern part is characterized by a steep dip. In general, the Abu Roash 'G' horizon generally dips to the northwest. Its depth ranges from 2000 m at the southeast to about 5200 m at the northwest (6). In general, lithofacies analysis revealed that this member is laid down across a relatively wide spectrum of depositional environments ranging from deltaic, intertidal, shallow subtidal to shoreface settings.

The Abu Roash 'G' Member is formed from limestone and shale, with the interbedding of sandstones. It also contains a dolomite member; this dolomite is thought to be deposited in a sabkha-type or a near-shore environment in the Alamein field (7). A core analysis done on the Abu Roash 'G' Member in the Karama oil field exhibited fair porosity and permeability values, where the lithology is primarily carbonate (dolomite and limestone) with some sandstone intercalation (8). In Abdo (7) it was said that the Abu Roash 'G' Member is of a near-shoreface environment, while in Saleh et al., (8) it was discussed that the Upper and Middle sections of the member are of a deltaic environment, and as for the Lower section, it was suggested that it is of a tidal complex environment.

In Assal et al., (9) the environment of the Upper unit of the Abu Roash 'G' Member was interpreted by using a core from the Sitra field, which is to the WNW of the West Qaroun oil field. Where the Upper unit of the Abu Roash 'G' Member was divided into the several sections depending on their sedimentary structures, for example: 1- the planer cross bedding + the massive sandstone will indicate a shoreface environment -2- the ripple lamination + the trough cross bedding will indicate a transitional environment between a tidal channel and the shoreface -3- bioturbation + shell debris will indicate a marine environment -4- the lenticular, wavy, and flaser beddings will indicate a tidal complex environment.

In Asala Ridge, Pasley et al., (10) reported that the sandstone interval of the Middle unit of the Abu Roash 'G' Member was said to be of a deltaic system, as for the Lower unit, it was said to be of a shallow marine environment, with some tidal influence. In Mira (11), the sand of the Middle and Lower units of the Abu Roash

'G' Member was said to be sand bars, based on the previous work done on the West Qarun field. In Sayed et al., (12), it was discussed that the Abu Roash 'G' Member in the Gabal Abu Roash area exhibited cross bedding with medium-coarse grained sandstone and biostrome.

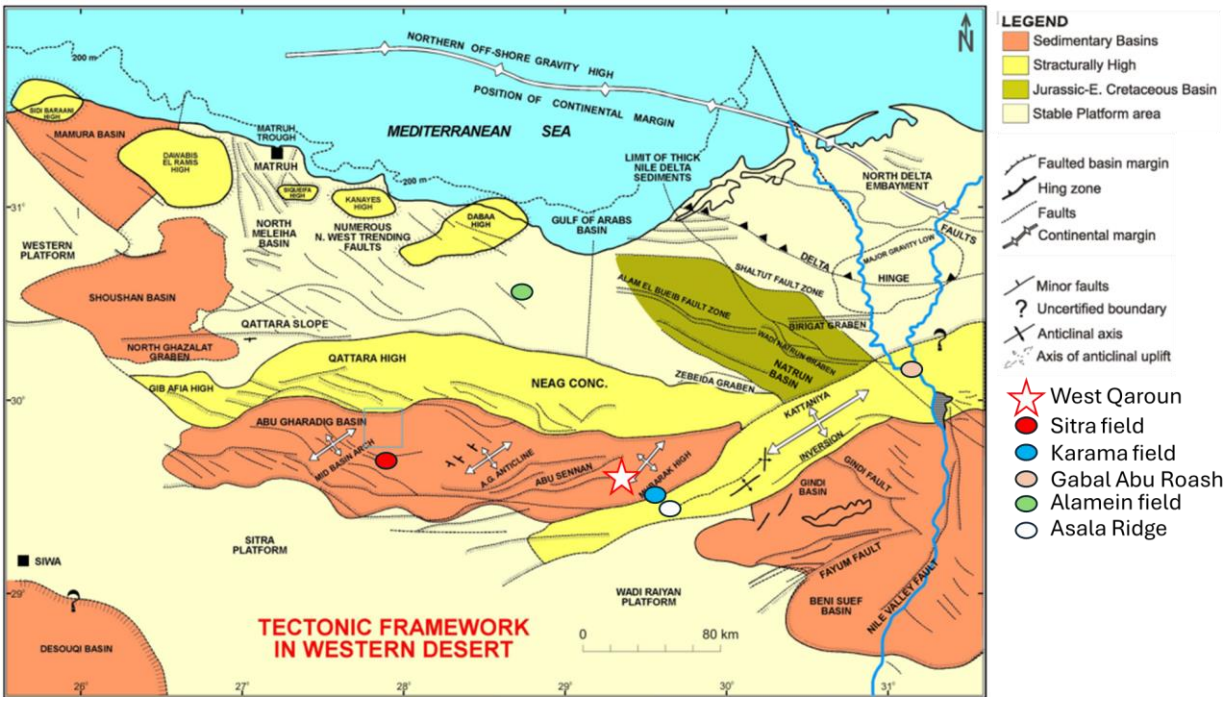

Fig. 2. The main structural divisions of the Abu Gharadig basin, modified after Bayoumi (13).

2. Data Availability

Four wells (WQ-9, WQ-10, WQ-23, and WQ-24) (Fig. 3) and their accessories of logs (Table 1), and formation tops with one Mud log report for each well.

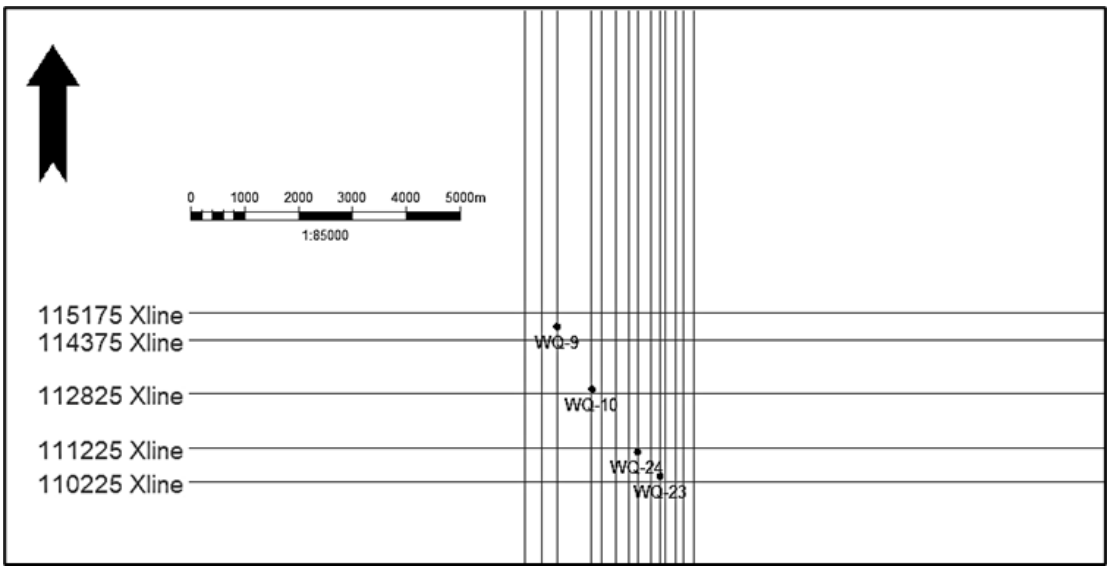

Fig. 3. The available 2D seismic lines and the four studied wells.

Table 1. The four wells and their accessories of logs.

	WQ-9	WQ-10	WQ-23	WQ-24
Gamma-ray	✓	✓	✓	✓
Total Porosity		✓	✓	✓
Effective Porosity		✓	✓	✓
Neutron	✓	✓	✓	✓
Density		✓	✓	✓
Deep Resistivity	✓	✓	✓	✓
Mudlogger Lithology	✓	✓	✓	✓
Water Saturation		✓	✓	✓
Photoelectric Factor		✓	✓	✓
Generated Lithology		✓	✓	✓

3. Lithology from Quanti-Elan (Eq)

Facies provide information about the depositional environments but do not define the sedimentological composition of a rock, which must be determined from core data or well logs. For example, sandstone indicates grain size but does not specify the composition; it may consist of quartz, oolitic limestone, or other sand-sized materials. Lithology is determined using Weatherford neutron versus density and photoelectric versus density plots (Fig. 4). The Abu Roash 'G' Member is predominantly limestone, followed by dolomite and sandstones. The cleanest intervals, with the lowest gamma-ray values, correspond to limestone, whereas the dirtiest intervals, with the highest gamma-ray values, correspond to dolomite. Sandstones exhibit intermediate gamma-ray responses.

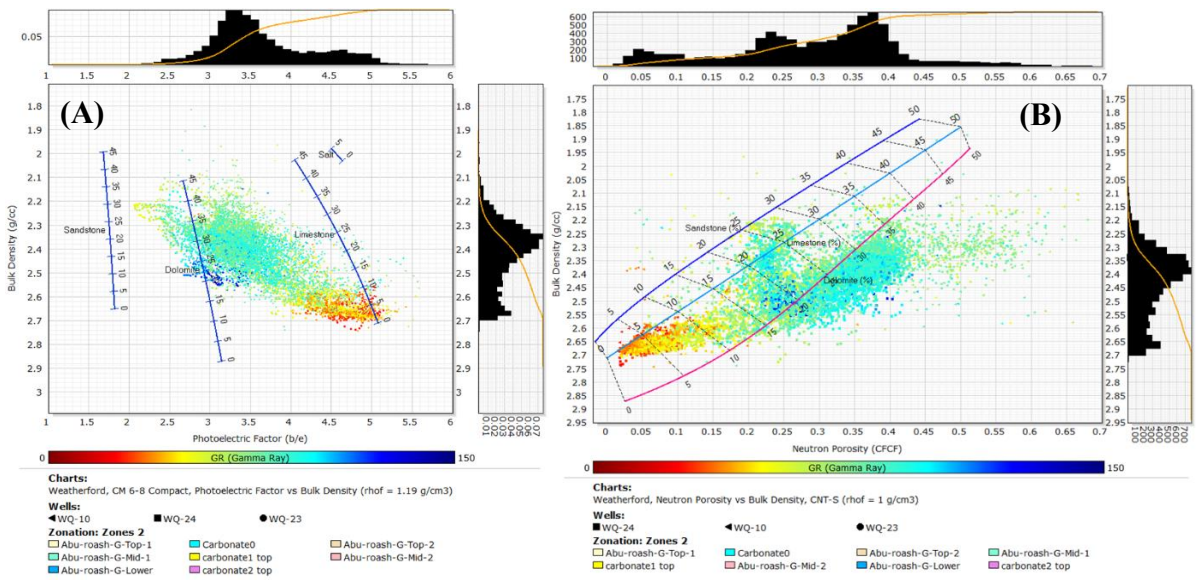

Fig. 4. (A) Weatherford Photoelectric Vs. Density plot. (B) Weatherford Neutron Vs. Density. with the range of lithologies of the Abu Roash 'G' Member.

The Quanti-Elan workflow employs the neutron porosity log, bulk density log, shallow and deep resistivity logs, and effective porosity log; however, these logs are unavailable for well WQ-9. The workflow generates lithofacies such as shale, quartz, and calcite, which serve as components for the lithology identifier algorithm. Using this approach, lithology identifier logs are created for wells WQ-10, WQ-23, and WQ-24, providing predicted lithologies that can be integrated to interpret facies.

A detailed analysis is implemented for each well to capture the heterogeneity. Figure 5 shows the gamma-ray of well WQ-9, representing a unimodal pattern and detailing the occurrence of a single environment. In addition, on the left side of the figure, a little bump in zone 1 signifies an intrusion in that homogeneous environment. From this pattern, it is concluded that there is a major shaliness modal that is skewed to the right side of the histogram in zones 2 and 3. A clean/non-shaliness minor modal is separately skewed to the right side of the histogram in zone 1.

Going to the SE direction to the WQ-10 well, values of gamma-ray of the Abu Roash 'G' Member become more homogeneous, i.e., unimodal, and less shaly than the values in the WQ-9 well. We can distinguish three zones representing separate ranges of gamma ray values, representing three lithological types (Fig. 6). Zone 1 documents the occurrence of the cleanest lithology (i.e., carbonates). Zone 2 represents a mix of sand and silt, while the composition of zone 3 is mainly shale.

The gamma-ray values of well WQ-24, in the Abu Roash 'G' Member, are greatly similar to those of well WQ-10 and to a lesser degree to those of well WQ-9 (Fig. 7). Values display a bimodal pattern but with less frequency of repetition in the high end of values. This histogram represents a cleaner, less shaly environment than that of well WQ-9 (Fig. 5). In zone 1, the percentage of sand is lower than in well WQ-10 (Figs. 6, 7).

Going to the SE direction to the WQ-23 well, values of gamma-ray of the Abu Roash 'G' Member are nearly identical to those of well WQ-24 (Figs. 7, 8). This matched relation can be explained by a noticeable short distance separating these two wells (Fig. 3). However, well WQ-23 exhibits a higher range of values in zone 2, and a larger separation between zones 1 and 2. This may confirm that well-23 has a finer grain size, moving from being silty in well WQ-24 to clay-sized sediments in well WQ-23. In summary, the northern and southern parts of the studied field have higher shale contents than the middle part. In other words, the middle part is cleaner and more homogeneous. It seems that we have a major depositional setting, including some minor environmental settings. Additionally, the effective porosity is also plotted, interpreted, and correlated. The PHIE values exhibit a significant decrease towards the south of the field.

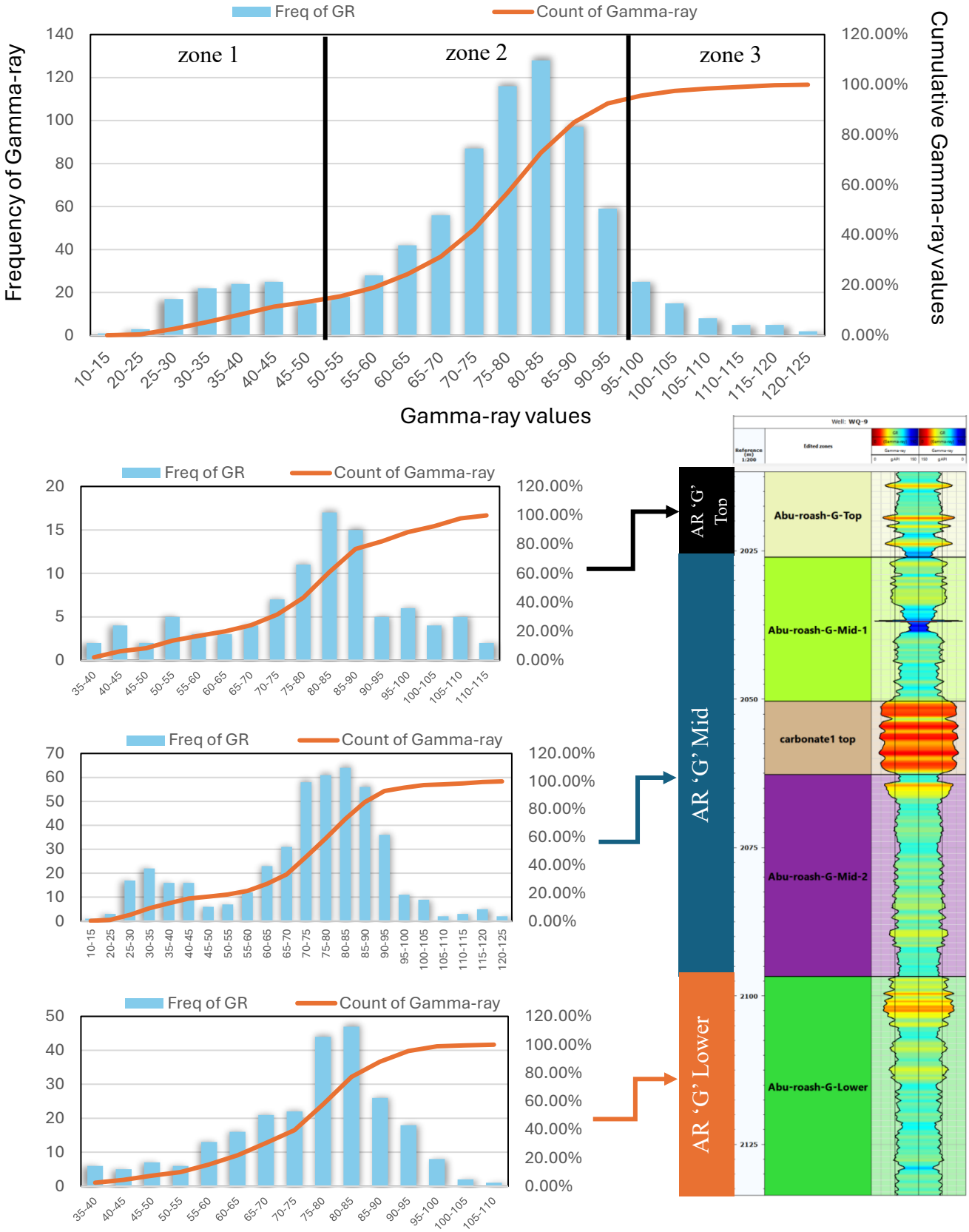

Fig.5. The gamma-ray histograms of the Abu Roash 'G' Member in the WQ-9 well.

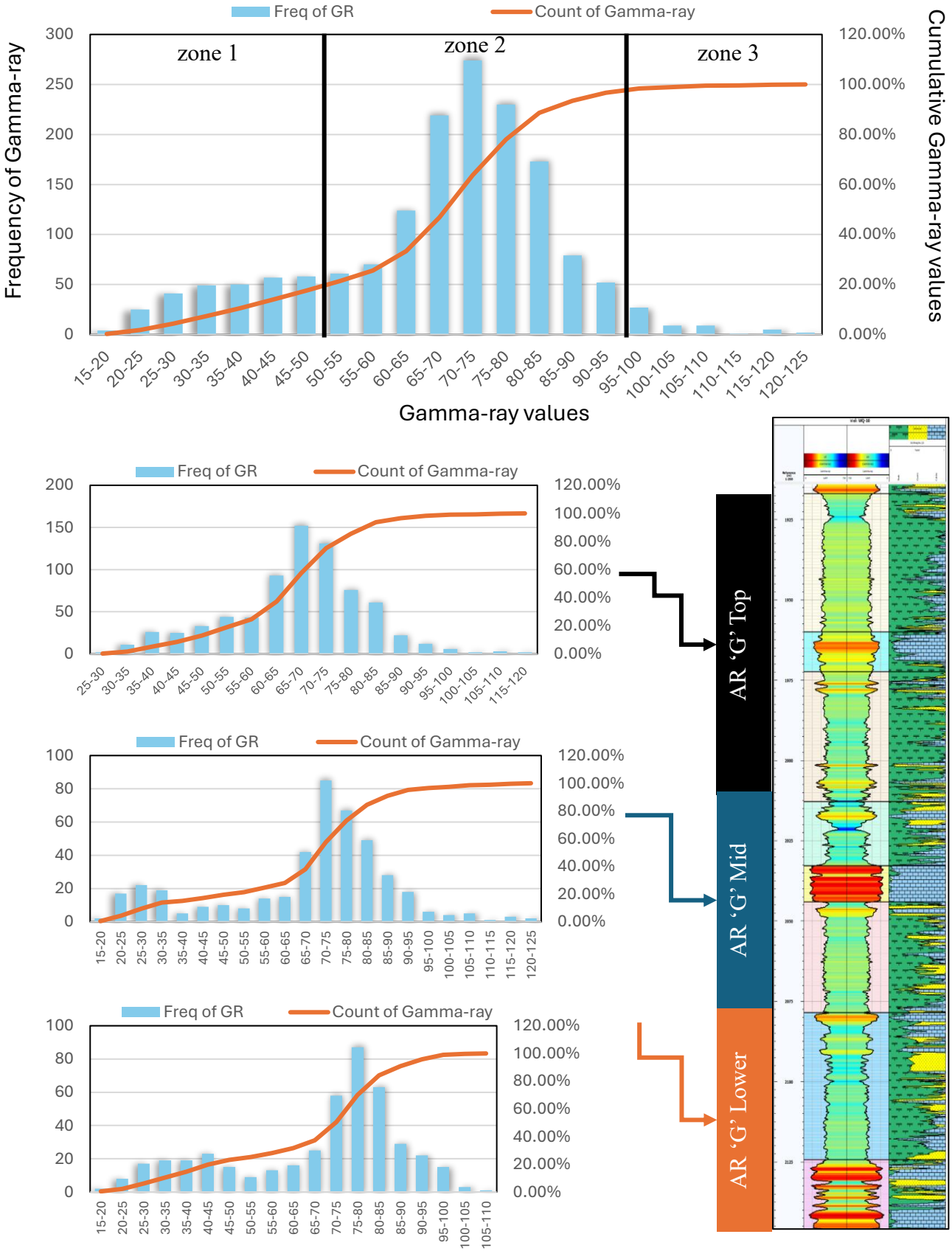

Fig.6. The GR mirror image and histogram of the Abu Roash 'G' Member in the WQ-10 well.

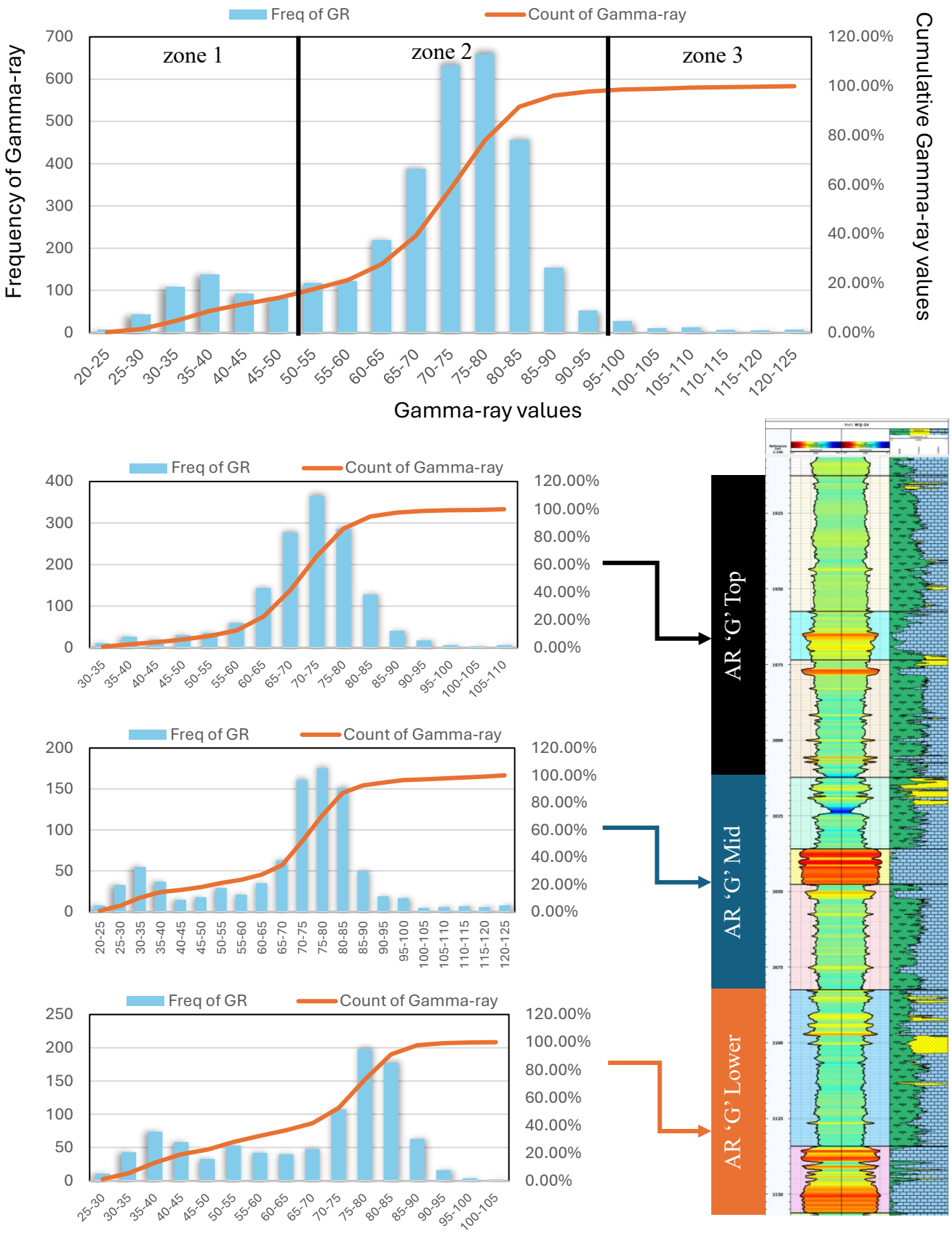

Fig.7. The GR mirror image and histogram of the Abu Roash 'G' Member in the WQ-24 well.

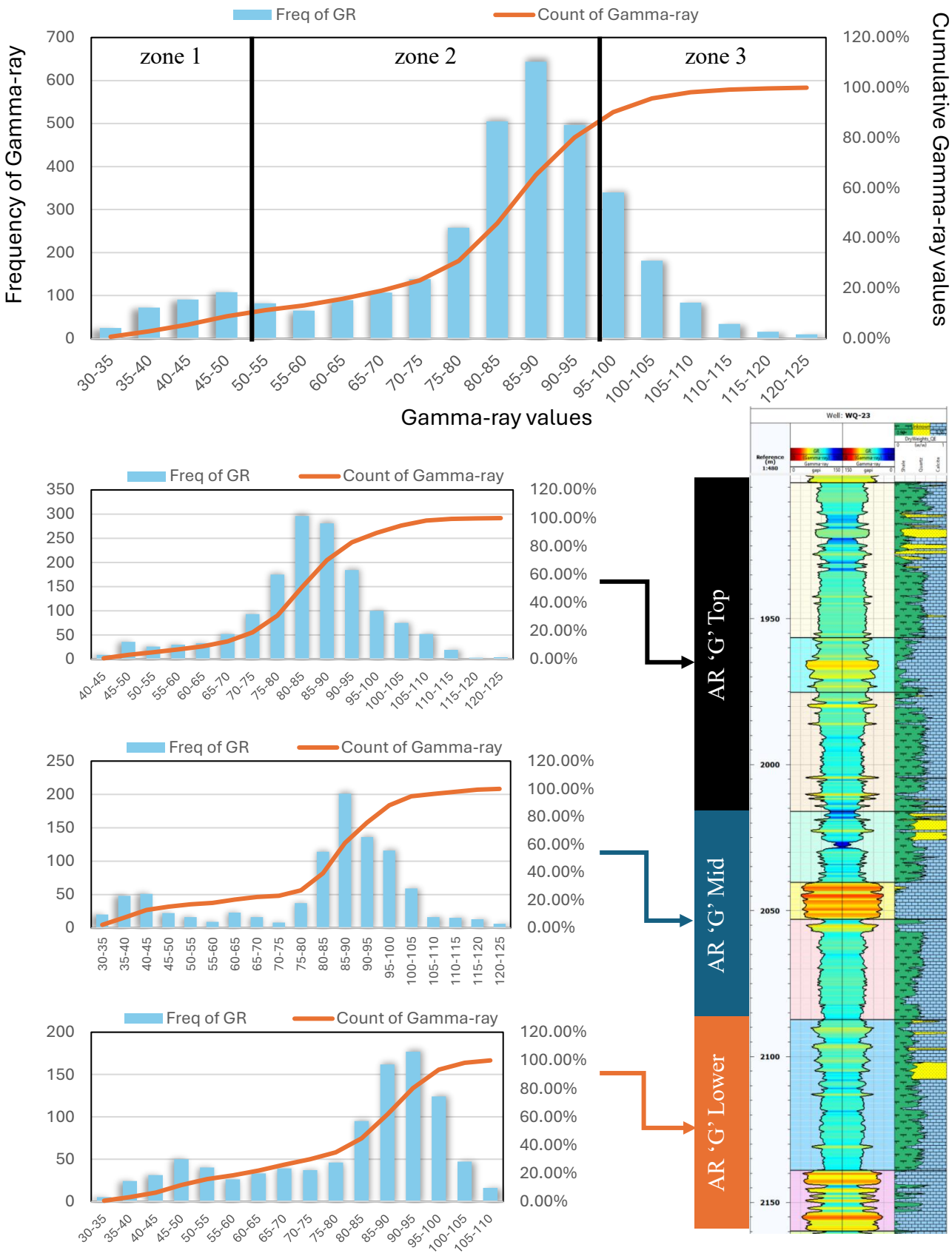

Fig.8. The GR mirror image and histogram of the Abu Roash 'G' Member in the WQ-23 well.

4. Facies from Electronic Well Logs

In the absence of core and FMI data, as in the present study, a technique that captures facies from electronic well logs, mainly based on the work of Emery and Myers (14) (Fig. 9), is decisive. In addition, Salah Abbas (personal communication) improved this technique using a gamma ray spectrometer to characterize each facies in a surface succession. Gamma-ray log shapes are commonly used by geologists to infer trends and subsequently depositional facies. Fluctuating energy levels are represented by a serrated or zigzagged line, while constant energy levels are represented by smooth curves or lines. In summary, the sharper the edges of the line, the greater the fluctuation differences.

- High readings of Gamma-ray values indicate shale (fine-grained, low-energy environments). Low readings suggest non-shale (high-energy environments).
- Bell shapes represent waning-current sequences, retrogradational settings.
- Funnel shapes imply upward-increasing energy and progradational settings.
- Cylinder shapes reflect relatively constant energy levels and aggradational settings.
- The smoothness of the gamma-ray line also indicates the fluctuation of energy levels.

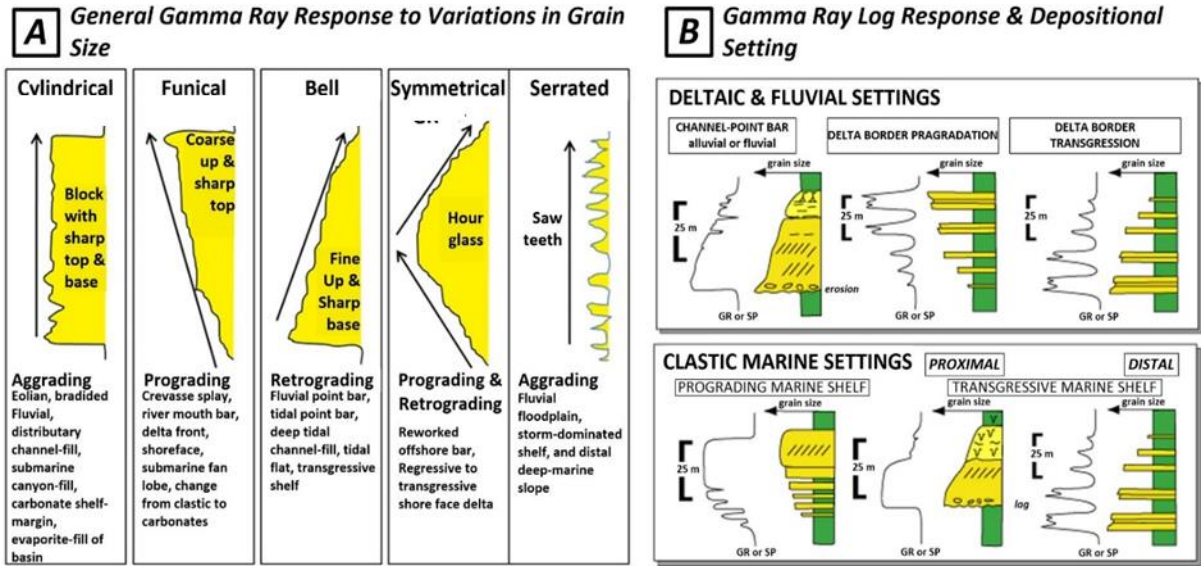

Fig.9. Gamma ray log response features and shapes for typical sedimentation. A: Emery and Myers (14) , B: Rider (15).

The facies log of the Abu Roash 'G' Member is constructed manually using the mirror-image log technique, which mirrors the same log across two tracks, e.g., (Fig.10). Well WQ-10 is used as the reference for the facies log, integrating the mirror-image logs, lithological mud logs. The integrated log suite from well WQ-10 provides a detailed record of the stratigraphic succession, revealing pronounced lithological heterogeneity and distinct variations in reservoir quality across multiple intervals. Figures (11-18) consist of eight sections with twelve logs: gamma ray, total and effective porosity, neutron, density, deep resistivity, mud-logger lithology, gas spikes, water saturation, photoelectric factor, and lithology. Where the colour scheme corresponds to the log values. The prescribed colour scheme for photoelectric factor log (orange for pure limestone/high calcite, dark green for shale, light green for shaly sand, yellow for quartz-rich sandstones).

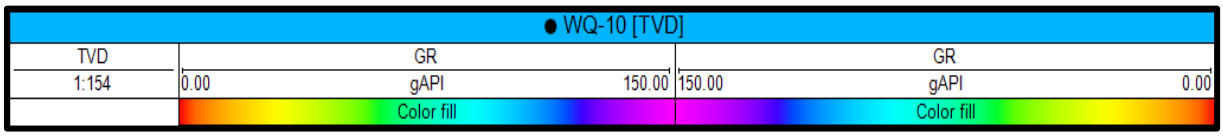

Fig.10. The header of the gamma-ray mirror image log.

The WQ-10 wireline panel documents a recurring succession of low-gamma carbonate intervals separated by thin argillaceous horizons that coincide with stratigraphic marker tops (Abu Roash 'G' tops; Carbonate 0, Carbonate 1, and Carbonate 2). Low gamma-ray values occur simultaneously with modest increases in bulk density and pronounced troughs on the total and effective porosity tracks. Effective porosity peaks where density decreases, often paired with moderate resistivity increases, implying the presence of a mixed pore system. These associations between porosity and resistivity are concentrated within the Abu Roash 'G' Mid-1, Mid-2, and Lower subdivisions.

Logged observations of "weak oil shows" correspond with several porosity maxima. The lithology tracks confirm a dominantly carbonate composition with thin argillaceous interbeds that act as intraformational seals. The vertical arrangement of clean carbonate units separated by argillaceous or micritic caps is consistent with deposition in a carbonatic shoreface ramp setting. Irregular porosity geometries and sharp density reductions indicate selective dissolution and the formation of moldic–vuggy porosity or localized dolomitization. Conversely, micrite, calcite cement, and pore-lining clays have occluded porosity in many low-gamma carbonate intervals, resulting in low effective porosity despite clean lithologies. Diagenetic heterogeneity thus governs both the magnitude of porosity and its contribution to fluid flow. A significant fraction of the total porosity is interpreted as bound or microporosity, which does not contribute to permeability. Applying a screening criterion of (PHIE ≥ 8–10% coupled with resistivity), isolates thin net-pay clusters centred at approximately 1,955–1,970 m (Mid-1), 2,020–2,035 m (Mid-2), and 2,060–2,080 m (Lower).

Beginning with the shallowest interval, the Abu Roash 'G' Top-1 (~1,703–1,740 m) is characterized by low gamma-ray values, indicative of clean lithologies. The photoelectric factor log records a reduction in orange zones with an increase in dark green intervals, signifying the presence of shales interbedded with carbonates. Total porosity ranges between 15–23%, with effective porosity tracking closely, reflecting high-quality reservoir facies with minimal clay content. Resistivity values are moderate, while water saturation remains high, suggesting water-wet lithologies with no significant hydrocarbon saturation, supported by elevated gas readings (Fig. 11).

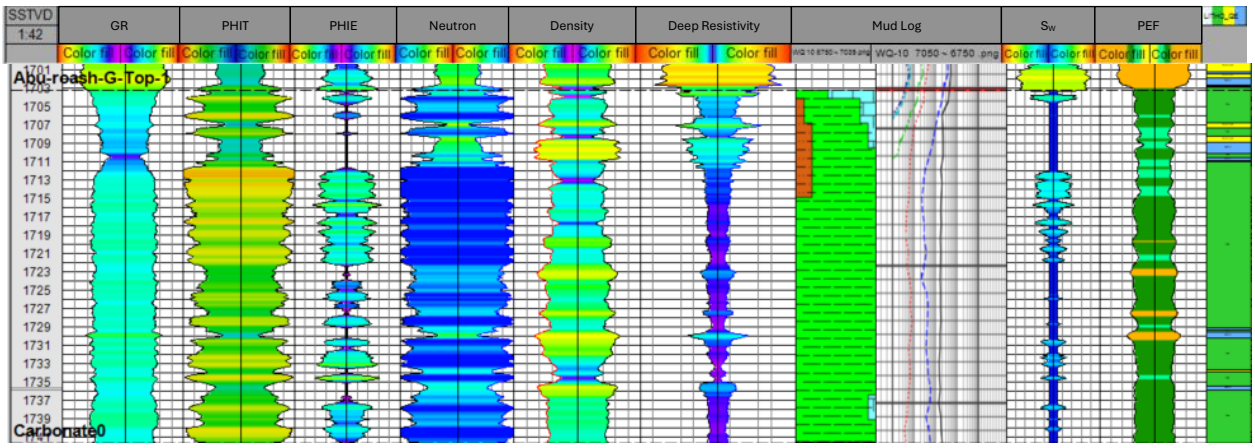

Fig.11. The created mirror images of Abu Roash 'G' Top-1, WQ-10.

In the Carbonate-0 interval (1,740–1,766 m), gamma-ray values fluctuate between 20 and 80 API. The photoelectric factor log indicates a mixture of orange (limestone), dark green (shale), and light green (sandy shale) intervals, suggesting alternating carbonate, shale, and quartz-rich sandstone lithologies, consistent with deposition on a carbonate shelf. Resistivity values increase noticeably, with strong gas peaks that indicate hydrocarbon presence. Water saturation decreases by ~0.3%. The neutron and density logs confirm gas-bearing intervals, enhanced by secondary porosity development within vuggy limestones (Fig. 12).

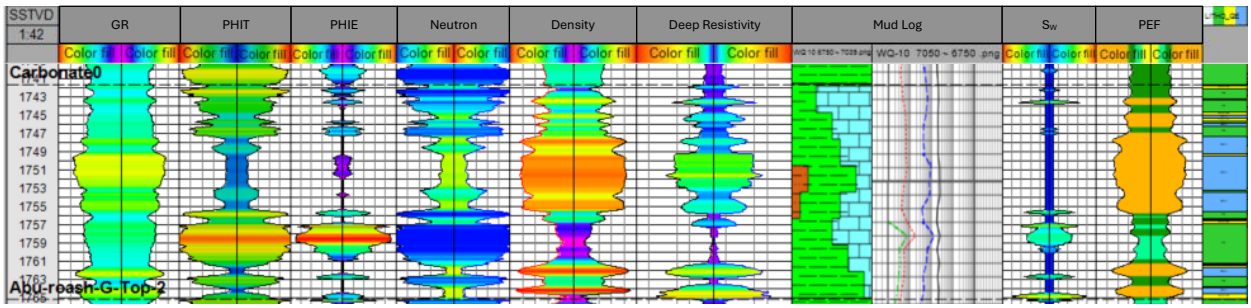

Fig.12. The created mirror images of Carbonate-0, WQ-10.

The Abu Roash 'G' Top-2 interval (1,766–1,800 m) shows gamma-ray values spiking to 60–70 API, with the photoelectric factor log recording an increase in dark green shaly horizons disrupting the orange carbonate zones. Porosity is heterogeneous (5–20%), resistivity decreases, water saturation increases, and gas shows diminish, indicating predominantly water-wet lithologies with minor hydrocarbon microseepage (Fig. 13).

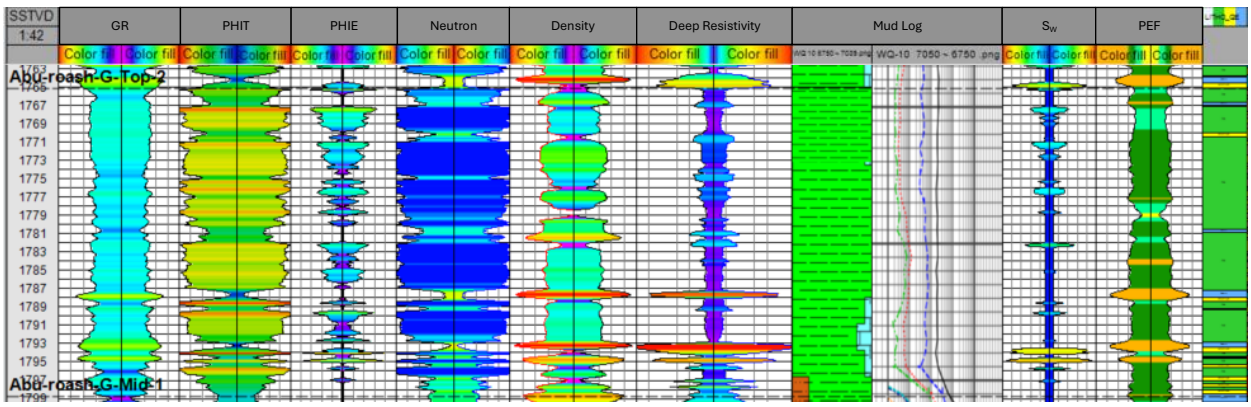

Fig.13. The created mirror images of Abu Roash 'G' Top-2, WQ-10.

The Abu Roash 'G' Mid-1 interval (1,800–1,820 m) is defined by high resistivity and low water saturation, paired with strong gas shows. Neutron and density signatures confirm their role as the most prospective hydrocarbon-bearing zone. The photoelectric factor log displays increasing light green and yellow intervals, reflecting the presence of quartz-rich components interbedded within carbonates (Fig. 14).

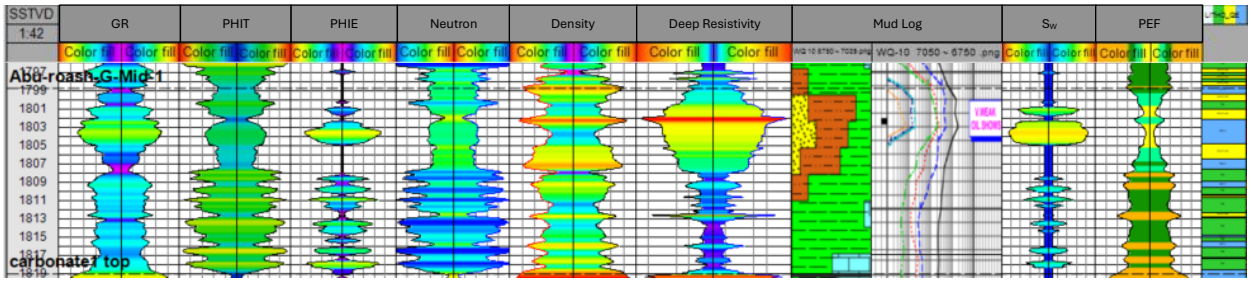

Fig.14. The created mirror images of Abu Roash 'G' Mid-1, WQ-10.

In the Carbonate-1 interval (1,820–1,835 m), the photoelectric factor log is dominated by orange coloration, indicating pure limestone and high calcite content. Gamma-ray values narrow into the 15–30 API range, consistent with clean carbonates, while porosity decreases substantially (Fig. 15).

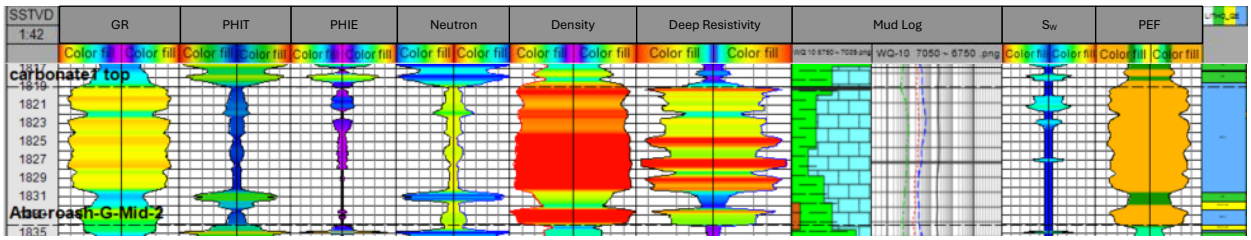

Fig.15. The created mirror images of Carbonate-1, WQ-10.

The Abu Roash 'G' Mid-2 interval (1,835–1,862 m) exhibits a sharp increase of gamma-ray values between 40 and 80 API. The photoelectric factor log transitions to dark green (shale) and light green (quartz-rich sandstones and shales) dominance, with limited orange carbonate representation. Porosity increases to 10–25%, while resistivity decreases and water saturation rises. Gas responses diminish, suggesting siliciclastic-rich, water-wet facies with poor reservoir potential (Fig. 16).

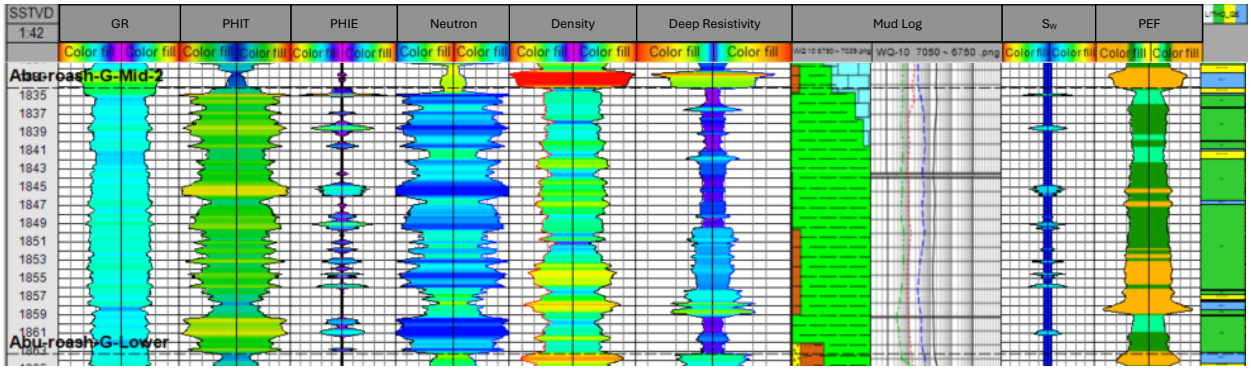

Fig.16. The created mirror images of Roash 'G' Mid-2, WQ-10.

The Abu Roash 'G' Lower interval (1,862–1,910 m) is marked by highly variable gamma-ray values (30–100 API) and photoelectric factor patterns dominated by dark and light green coloration, confirming siliciclastic dominance with alternating shale and sandstone. Porosity ranges between 5–25%, resistivity is moderate, and water saturation is consistently high, supporting a non-hydrocarbon-bearing interpretation (Fig. 17).

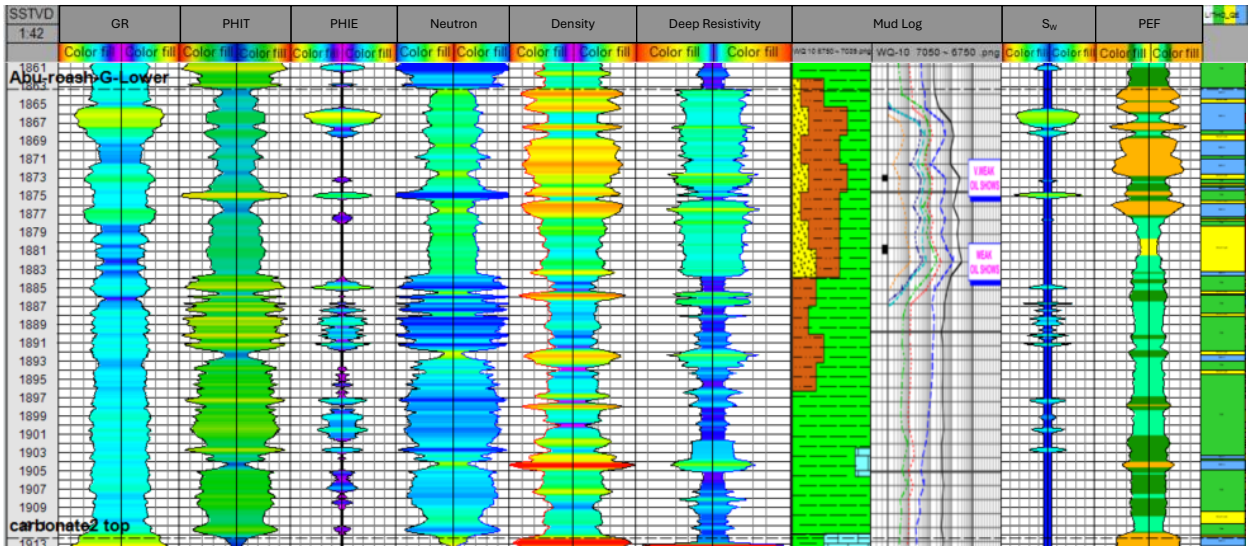

Fig.17. The created mirror images of Abu Roash 'G' Lower, WQ-10.

Finally, the Carbonate-2 interval (1,910–1,931 m) is characterized by dominant orange coloration on the photoelectric factor log, reflecting clean, calcite-rich limestone with limited sand input. Gamma-ray values are low (15–30 API), and effective porosity decreases significantly, indicating a tight, non-reservoir carbonate package (Fig. 18).

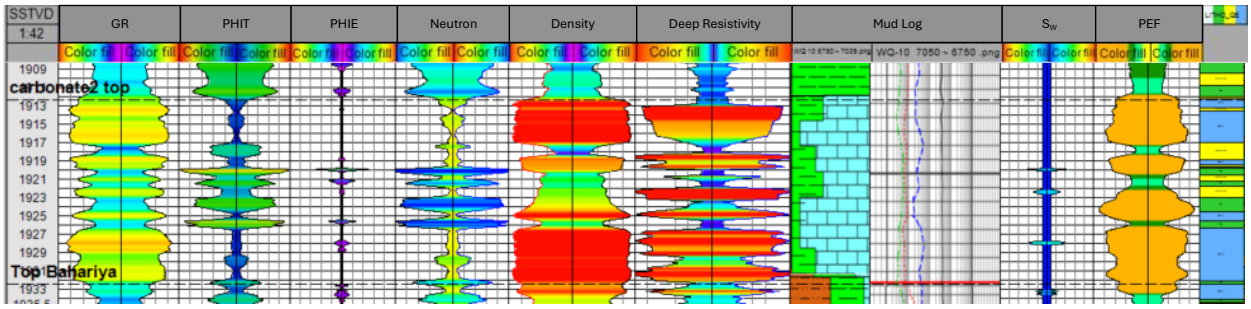

Fig.18. The created mirror images of Carbonate-2, WQ-10.

Seven facies are identified: Sand flat, Mixed flat, Mud flat, Dolomite, Upper Shoreface Carbonate, Upper Shoreface Sand, and Middle Shoreface Silt (Fig.19,20). This concept was based on the regional and known environmental composition of the Abu Roash 'G' Member, the surrounding known oil fields that are published, and the high fluctuation levels of the electronic well logs in the present study. From figures (5-8, 11-18), it is concluded that there is a major environment that is influenced by a lesser environment. The major environment exhibits cylinder shapes and aggradational settings, while being influenced by high fluctuation (serrated or zigzagged) settings. This leads to the conclusion that the environment is mainly of the shoreface setting, and that it is influenced by the tidal environmental setting

Code	Name	Parent	Background	Lines	Pattern
0	REMOVE				
1	Sand Flat				
2	Mixed Flat				
3	Mud Flat				
4	Dolomite				
5	U. Shoreface Carb				
6	U. Shoreface Sand				
7	M. Shoreface Silt				

Fig.19. The created facies for the Abu Roash 'G' Member.

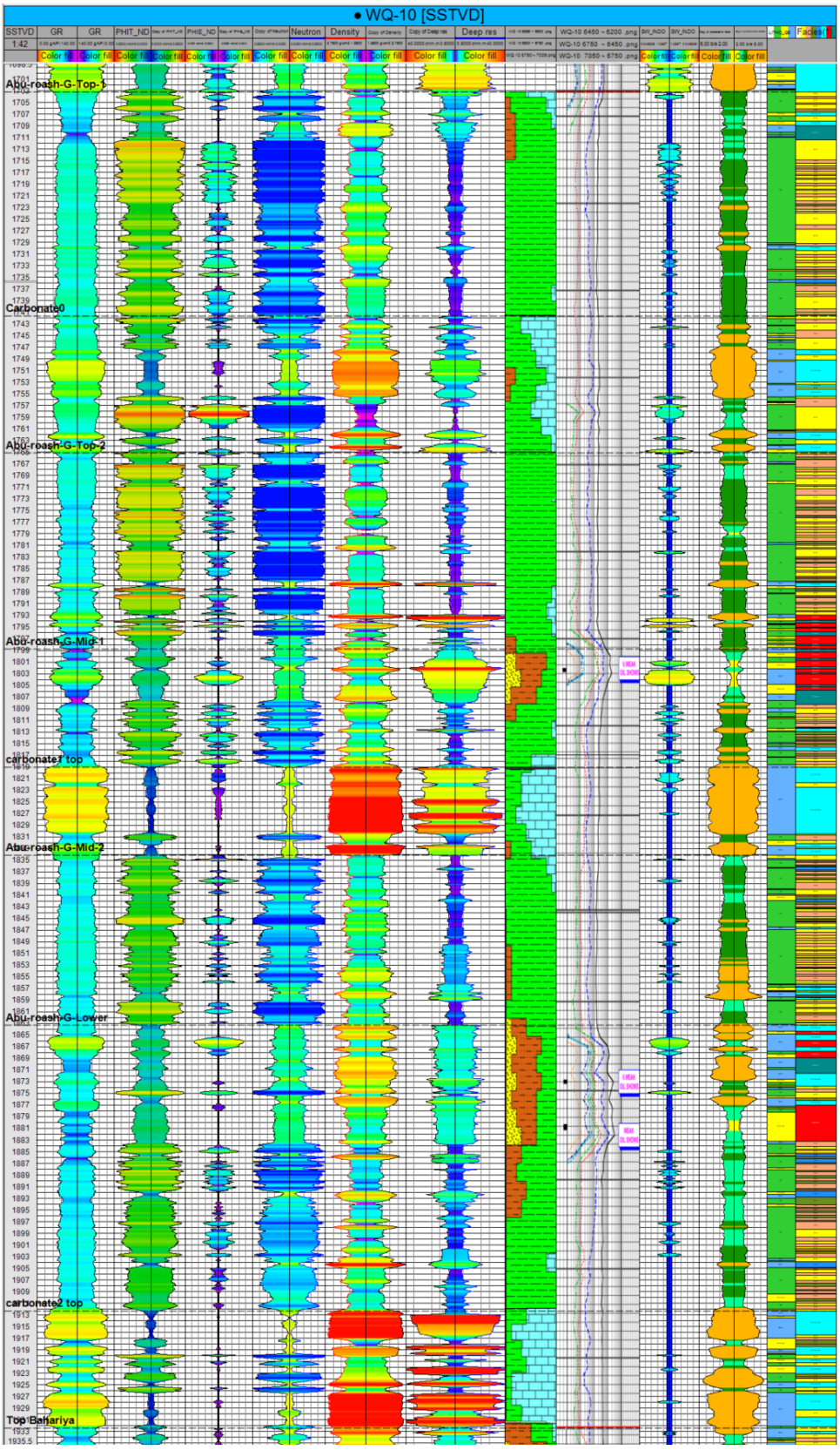

Fig.20. The created mirror images, mudlog, gas spikes, lithological log, and facies log for well WQ-10.

The integrated log suite from well WQ-9 is shown in Figure 21. The panel includes gamma ray, neutron, deep resistivity, mud-logger lithology, and gas spikes. So the facies control relies on the gamma-ray, since well WQ-9 lacks many logs.

The integrated log suite from well WQ-23 (Fig. 22) reveals two major hydrocarbon-bearing sandstone reservoirs separated by a tight carbonate. The gamma-ray log shows clean, low values (15–30 API) in the sands and higher readings (60–90 API) in shaly interbeds. The photoelectric factor log highlights orange carbonate zones acting as seals, with yellow and light-green signatures marking quartz-rich sandstones. Porosity is good, with total and effective values averaging 12–18% in the clean sands, while the carbonate remains tight (<5). High resistivity coincides with low water saturation and strong mud-gas spikes, confirming hydrocarbon charge. The stratigraphy reflects the tidal environment and shoreface deposition.

The integrated log suite from well WQ-24 (Fig. 23). records a mixed clastic succession with frequent argillaceous incursions relative to adjacent wells. The panel exhibits repeated high-gamma packages with dark-green photoelectric factor responses that correspond to shale-rich intervals tied to the Abu Roash 'G' marker tops. These units bound thinner, cleaner beds expressed by reduced gamma ray and light green to yellow. Within the cleaner beds, total porosity locally increases but effective porosity often lags, indicating appreciable clay-bound pore volume.

Resistivity is only moderate, and water saturation remains high, yielding a predominantly water-wet interpretation. Light-green/yellow photoelectric factor belts accompanied by modest density decreases and small effective-porosity peaks suggest quartz-rich sand lenses deposited within intertidal to upper shoreface settings. Yet muted resistivity and weak mud-gas spikes imply brine charge. Thin orange photoelectric factor streaks, where present, represent tight calcitic beds that further compartmentalize the section. Diagenetically, scarce dissolution features are noted where density troughs and slight porosity bulges occur within otherwise light green sands (Fig. IV.23). Well WQ-24 differs markedly from the others, being dominated by shale and water-wet sands with weak gas responses.

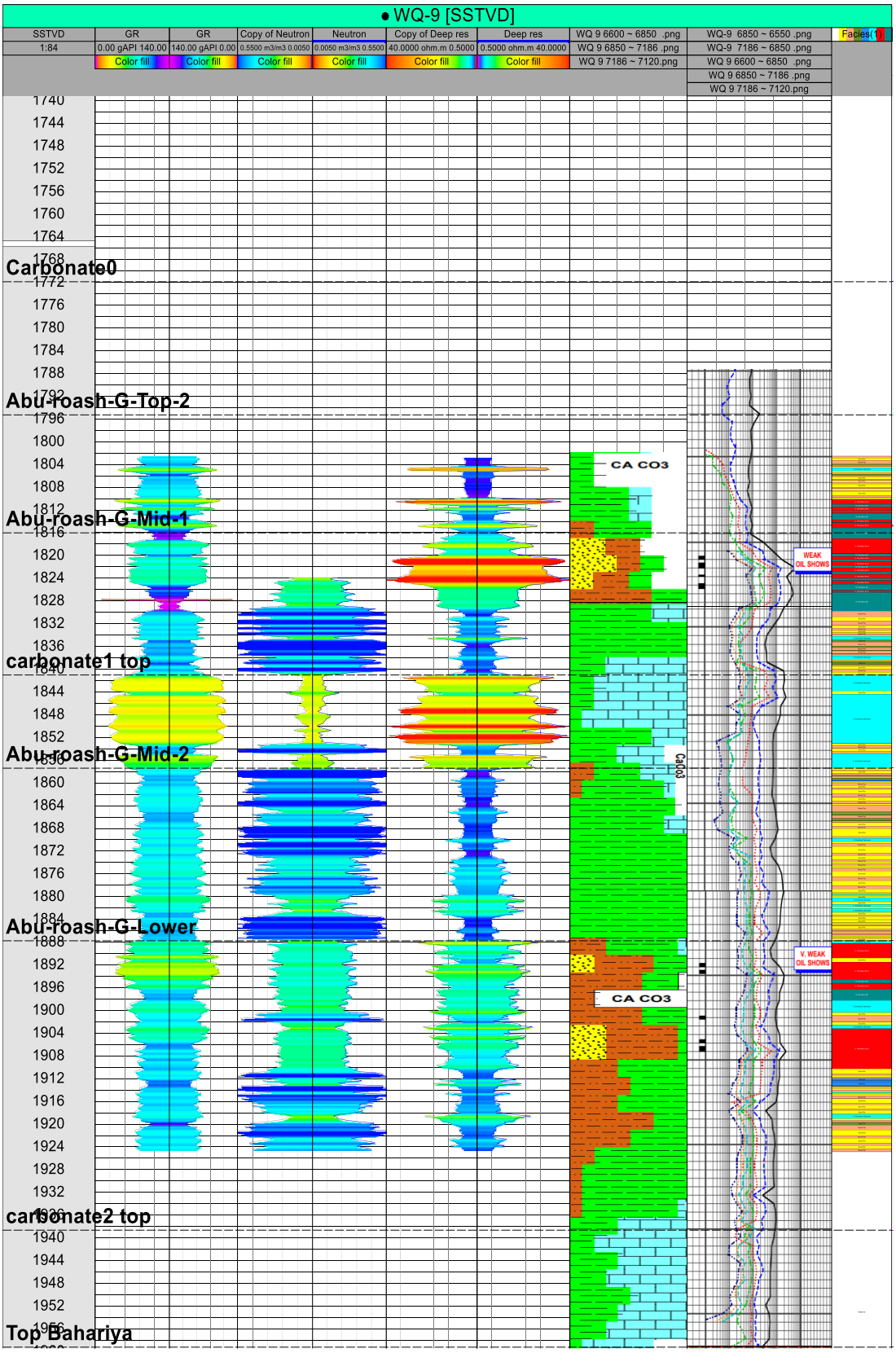

Fig. 21. The created mirror images, mudlog, gas spikes, lithological log, and facies log for well WQ-9.

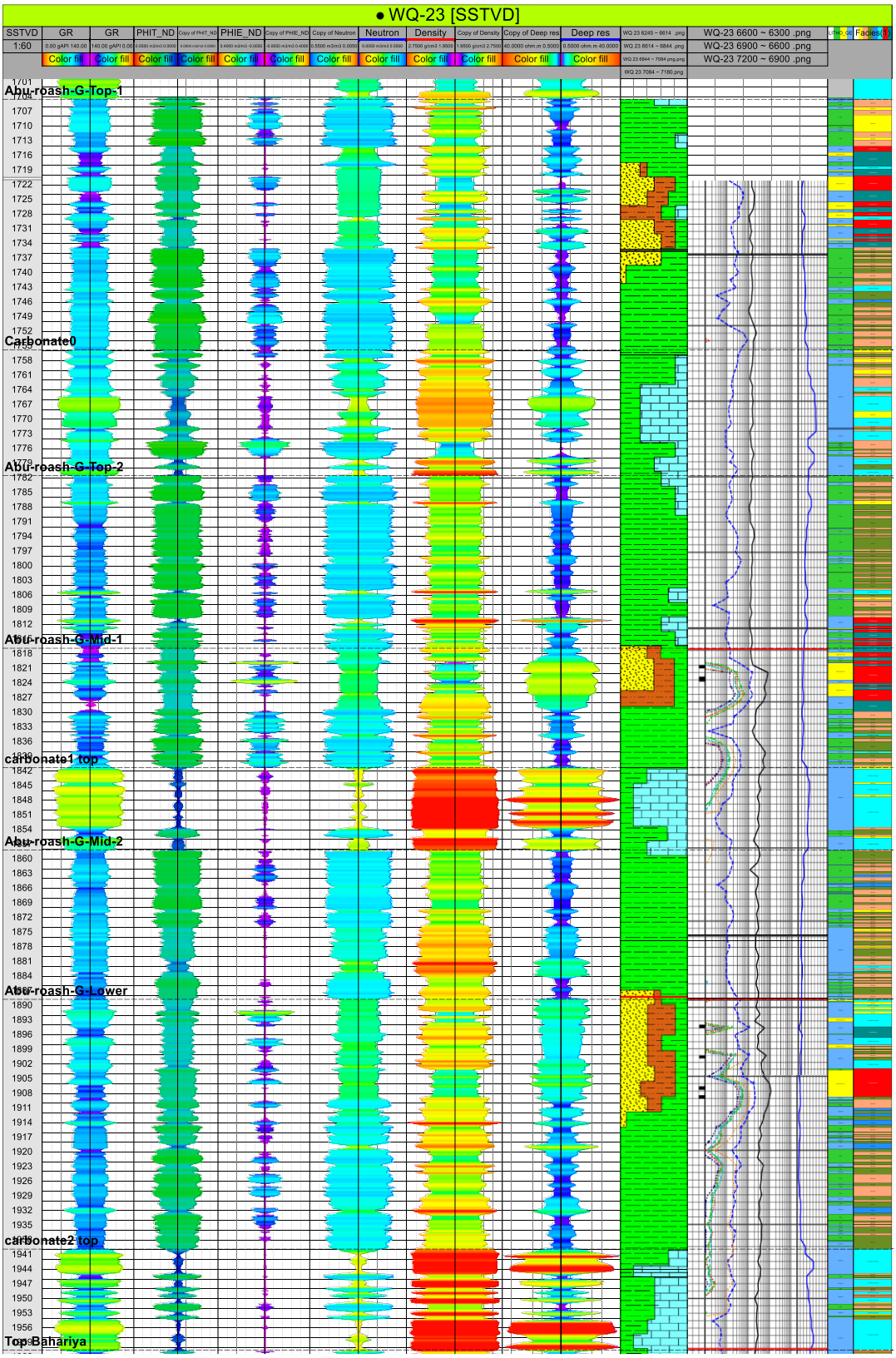

Fig. 22. The created mirror images, mudlog, gas spikes, lithological log, and facies log for well WQ-23.

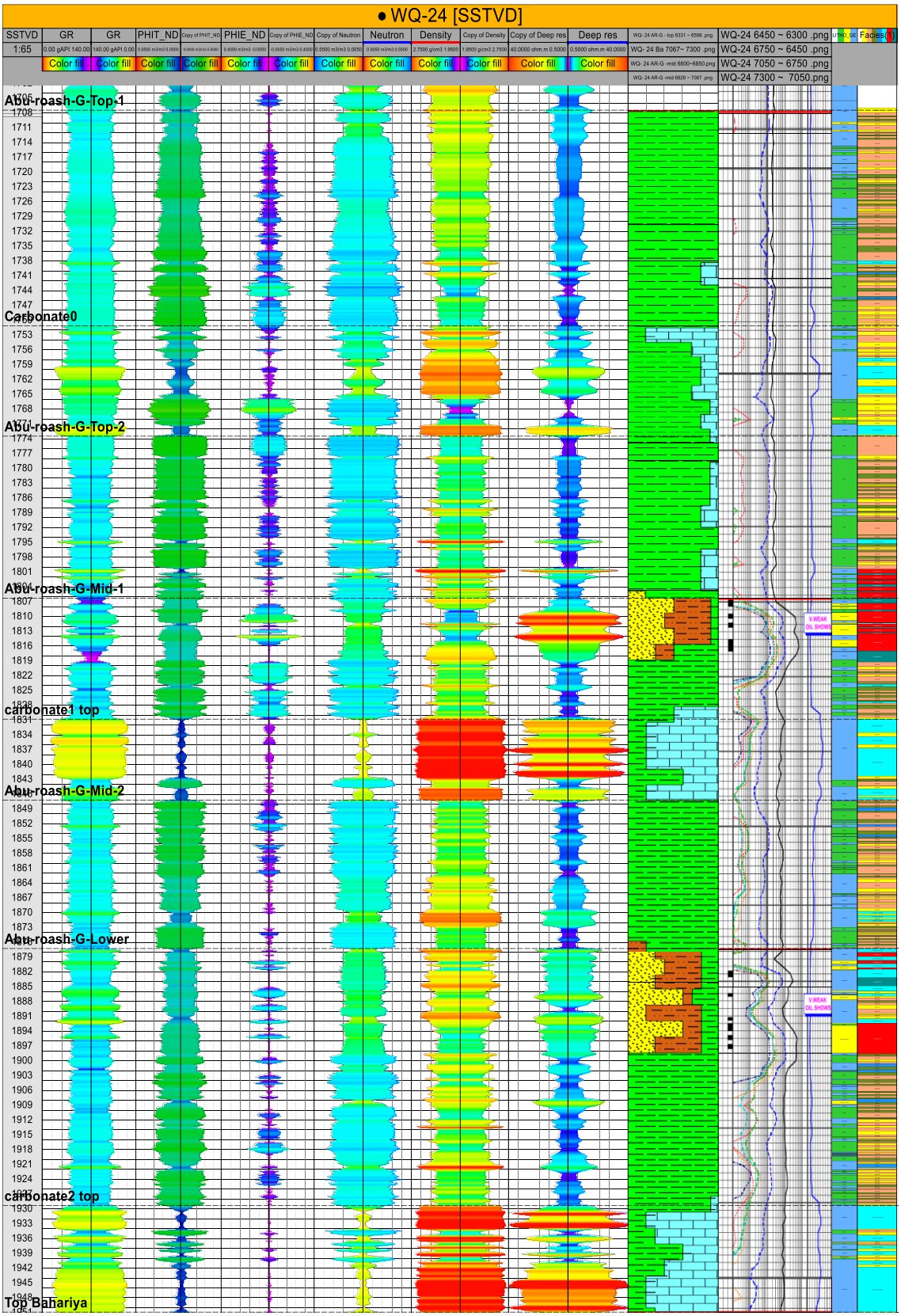

Fig. 23. The created mirror images, mudlog, gas spikes, lithological log, and facies log for well WQ-24.

5. Quality Control for the Proposed Facies Log

To check the quality of the interpreted facies log, crossplots are created. The crossplots' purpose is they show cluster separation between different facies. That is done by using the facies as the legend colour code. The density-photoelectric crossplot shows three clusters (Fig. 24), suggesting three distinctive environments. Each environment with characteristic criteria. For example, cluster (1) is characterized by high density, high photoelectric, and low gamma ray values, suggesting the upper shoreface carbonate facies.

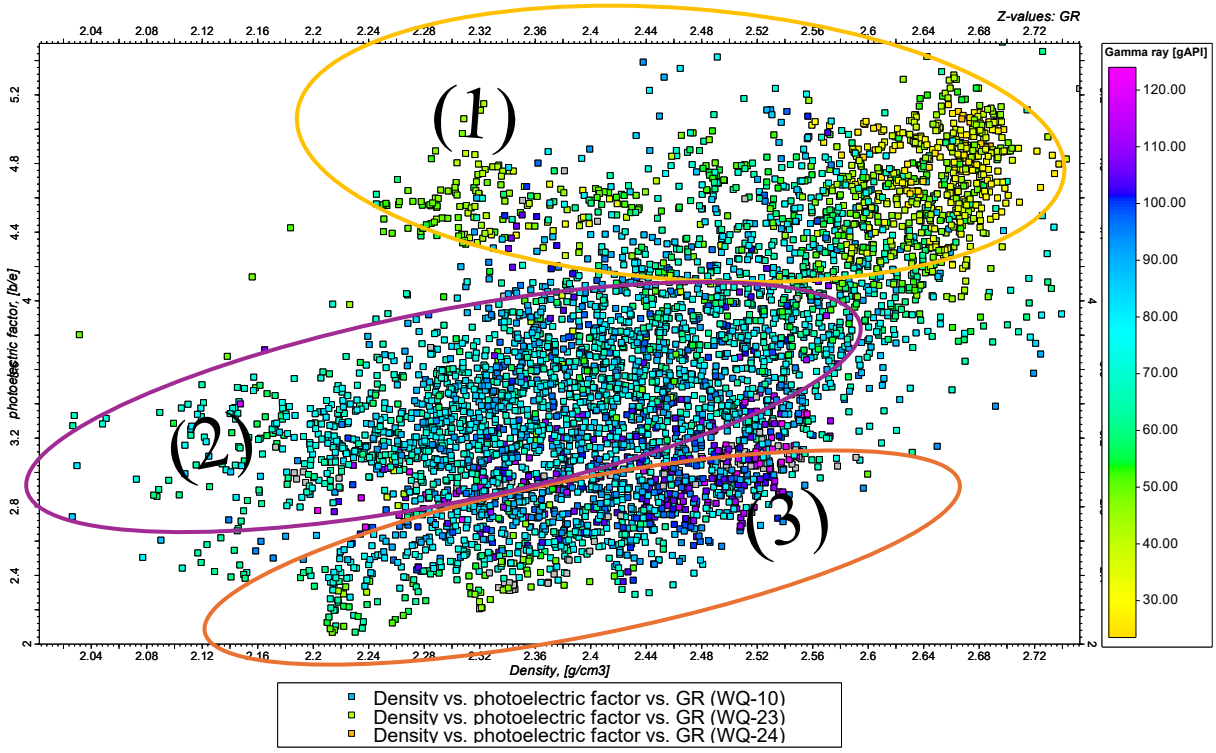

Fig.24. The density-photoelectric crossplot of the Abu Roash 'G' Member across wells (WQ-10, WQ-24, WQ-23), with the gamma-ray as legend.

The density-photoelectric crossplot shows the differences between the tidal flat and shoreface facies (Fig. 25). The tidal flat facies (Fig. 25A&B) show a wide distribution range and are very dense due to their thin laminae and cross-bedding bundle sequences. In contrast, the shoreface facies (Fig. 25A &C) have a clear separation between them and are characterized by a massive thickness with almost constant values. Note that the point size represents the effective porosity and the colour gradient denotes the facies.

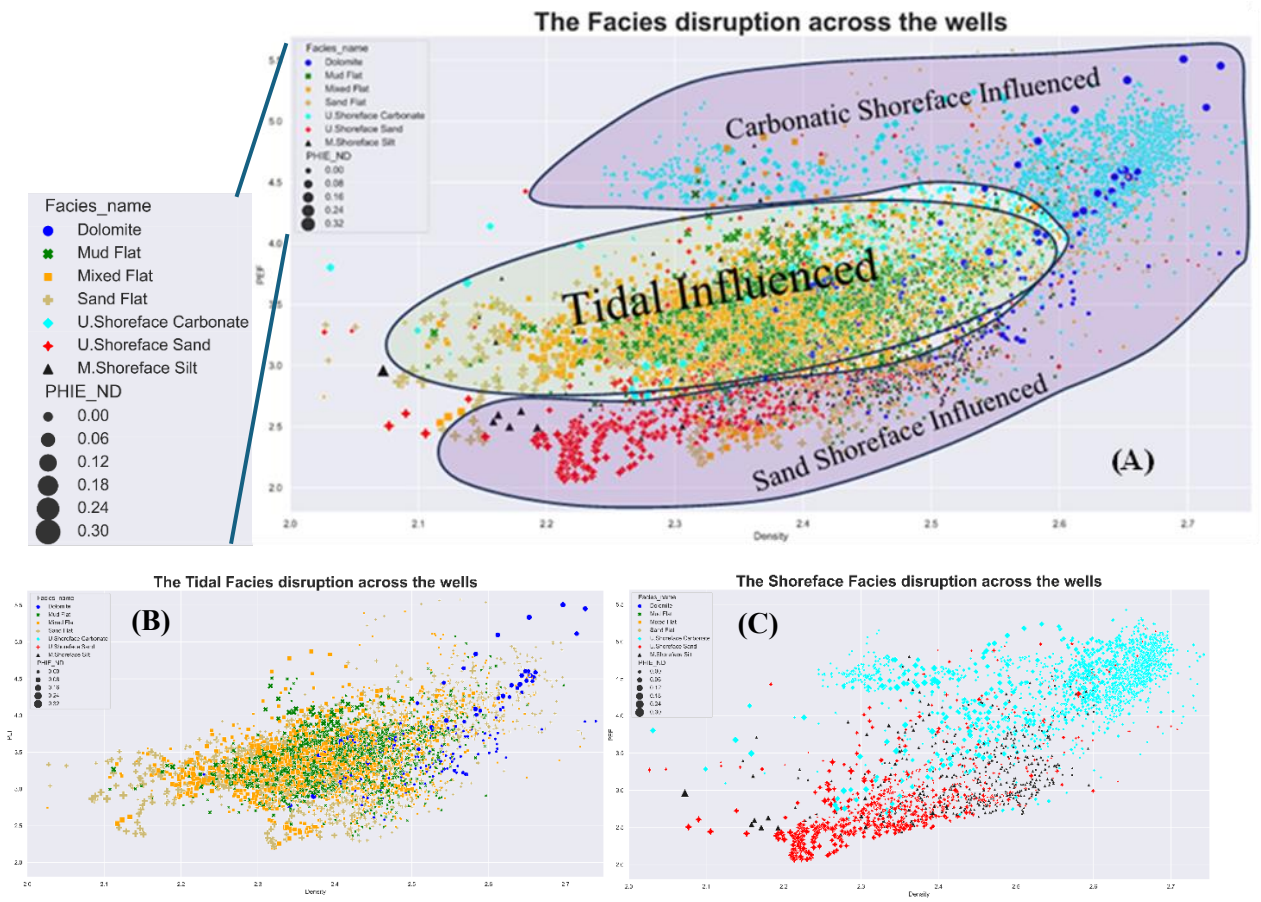

Fig.25. The density-photoelectric crossplot of: (A) Entirety of the Abu Roash 'G' Member. (B) Tidal flat facies of the member. (C) Shoreface facies of the member.

After trying many other scatterplots, only four showed significant separation between the clusters, making them important for quality checking. The scatterplots were:

1. The photoelectric on the X-axis and the micro-resistivity on the Y-axis (Figs. 26 [A]).
2. The shale volume on the X-axis and the neutron on the Y-axis (Figs. 26 [B]).
3. The photoelectric on the X-axis and the shale volume on the Y-axis (Figs. 26 [C]).
4. The total porosity- on the X-axis and the shale volume on the Y-axis (Figs. 26 [D]).

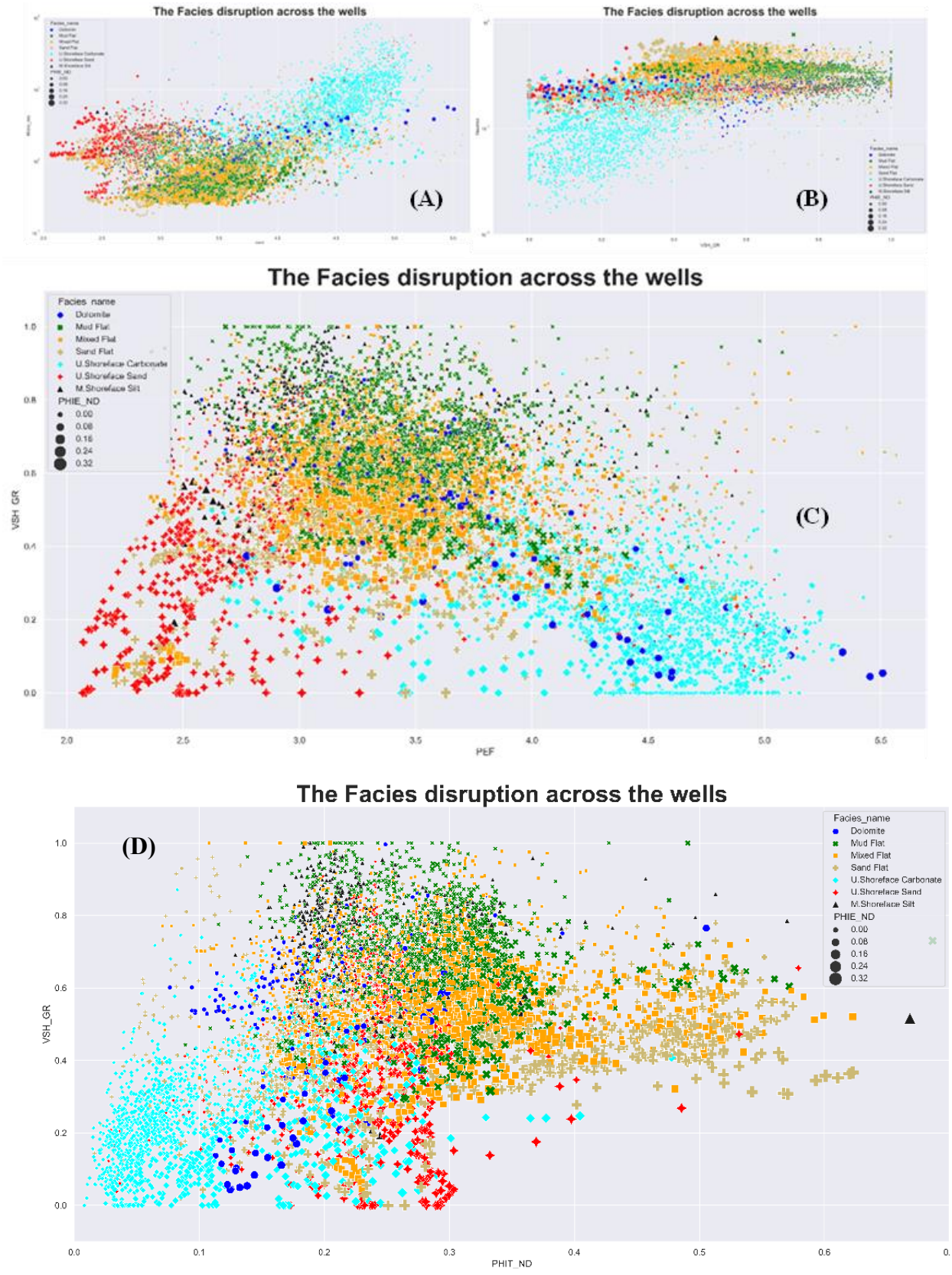

Fig. 26. The facies distribution across different plots (A, B, C, D).

6. Conclusion

All those plots prove and provide evidence that the facies created using the idea of patterns across different electronic well logs is accurate and dependable, but there are some criteria that should be met before using this technique. Firstly, the subsurface formation being modelled must have a surface type locality or core slab studies that are published for review. Secondly, the surrounding fields must be used as a reference to interpolate the paleoenvironment of the formation for accuracy. The mirror image technique is powered by its ability to provide and create patterns from electronic well logs; this ability is not just limited to the gamma-ray log, but it could also be used in all logs.

In the case of this study, the main lithology of the Member was carbonatic. This made the gamma-ray log incapable of reading the heterogeneity of the Member, which led to complications while correlating the wells with each other. But by creating and visualising patterns across different electronic well logs, it becomes possible to have high-accuracy correlations based on the facies created from the technique.

Conflict of interest: NIL

Funding: NIL

References

1. El-Behairy A, SPE, Abdel-Nabi M, Rizk M, Abdel-Moneim E, (SOG)_Sahara_Oil_and_Gas. Rejuvenation of West Qarun Field. Soc Pet Eng. 2013;(April):15–7.
2. Smith christopher M, Arbona P, Awad M, Chaffe W, Rehman C. Well Evaluation Conference, Egypt. In Schlumberger; 1984.
3. THE EGYPTIAN GENERAL PETROLEUM CORPORATION. Western Desert, Oil and Gas Fields (A Comprehensive Overview). Journal of Chemical Information and Modeling. THE EGYPTIAN GENERAL PETROLEUM CORPORATION; 1992. 449 p.
4. Said R. The Geology of Egypt [Internet]. Elsevier Publishing Company [distributors for the U.S.: American Elsevier Publishing Company, New York]; 1962. Available from: https://books.google.com.eg/books?id=RagJAQAAIAAJ
5. Egypt ministry of petroleum and Mineral. Egypt_Concession_Map [Internet]. 2023. p. 1. Available from: https://eug.petroleum.gov.eg/dp/pages/customcode/MDS_iTabs/information-img/Egypt_Concession_Map.pdf
6. Hassan NM, Hammouda H, Mohammed HF. Seismic Evaluation of the Subsurface Structural Setting in West Qarun Area, Western Desert, Egypt. 1997;(March 1997):21–44.
7. Abdo AAI. Petrophysical Characteristics and Hydrocarbon Occurrences of Abu Roash-G Dolomite, Alamein Field, Northern Western Desert, Egypt. Faculty of Science, Alexandria University; 2015.
8. Saleh AH, Farag AE, Eysa EA. Reservoir quality of Abu Roash (G) member in Karama Oil Field, East Bahariya Concession, North Western Desert, Egypt. Arab J Geosci. 2021;14(3).
9. Assal EM, Selim ESI, Hedaihed SM. Facies analysis, depositional architecture, and sequence stratigraphy of the upper Abu Roash "G" Member (Late Cenomanian), Sitra Field, Western Desert, Egypt. Arab J Geosci. 2021;14(12).
10. Pasley MA, Artigas G, Nassef O, Comisnky J. Depositional Facies Control from Reservoir Characteristics in the Middle and Lower Abu Roash " G " Sandstones, Western Desert, Egypt. In: Search and Discovery Article. 2009.
11. Mira A, El-Behairy A, El-Rahman MMA, Naby MA, Rizk M. Generic Approach of Integrating Core Data, and Petrophysical Interpretation to Generate Reliable Facies Model in Absence of Seismic Attribute Analysis- West Qarun Field Case Study. Soc Pet Eng - SPE North Africa Tech Conf Exhib 2015, NATC 2015. 2015;(1):792–807.

12. Sayed F, Hammed MS, Hussein AW, Shided AG. Surface expression of the Syrian Arc Kattaniya inverted basin in the Abu Roash area, northeast Western Desert, Egypt: Structural style and tectonic history. Mar Pet Geol [Internet]. 2020;117(April):104401. Available from: https://doi.org/10.1016/j.marpetgeo.2020.104401
13. Bayoumi T. The influence of interaction of depositional environment and syn sedimentary tectonics on the development of some Late Cretaceous source rocks, Abu Gharadig bash, Western Desert, Egypt. In: Proc EGPC 13th petrol Expl Prod Conf, Cairo, Vol II. Cairo; 1996. p. 475–96.
14. Emery D, Myers K. Sequence Stratigraphy. Encyclopedia of Earth Sciences Series. Blackwell Publishing Company; 1996. 1–297 p.
15. Rider M. The Geological Interpretation of Well Logs. Second. Rider-French Consulting Ltd, 2002. 290 p.